Published in IET Microwaves, Antennas & Propagation
Received on 13th February 2011
Revised on 23rd March 2011
doi: 10.1049/iet-map.2011.0089

ISSN 1751-8725

Periodically structured thin-film cables

R.R.A. Syms K. Segkhoonthod I.R. Young

Optical and Semiconductor Devices Group, EEE Department, Imperial College London, Exhibition Road, London SW7 2AZ, UK
E-mail: r.syms@imperial.ac.uk, r.syms@ic.ac.uk

Abstract: Periodic structuring of the ground plane is presented as a method of adjusting the properties of thin-film microstrip cables. Such cables may be useful as interconnects when flexibility is required and space is at a premium. Simple analytic models are presented and verified by numerical simulation. Prototype cables are fabricated in 2 m lengths of copper-clad polyimide. The effect of dimensions on characteristic impedance, cut-off frequency and propagation loss is investigated, and it is shown that impedance close to 50 Ω may be combined with low loss, using feature sizes compatible with flexible printed circuit board (PCB) fabrication.

1 Introduction

Well-known arrangements for signal routing on planar substrates include microstrip [1], co-planar waveguide (CPW) [2] and slot-line [3]. For uniform structures, conductor dimensions and substrate thickness and permittivity control the characteristic impedance [2–4]. Consequently, dimensional or material limitations may make it difficult to combine the desired velocity or impedance with low propagation loss. Methods of lumped element loading have therefore been developed to reduce circuit size [5, 6] or attenuation [7]. Periodic electrical structures have of course long been of interest (see e.g. [8]). However, periodic modification of continuous guides attracted only limited attention [9–11] until the rise in interest in photonic bandgap (PBG) devices. Modification of the signal or ground conductor can each give rise to multiple propagating bands, and filters have been developed in microstrip [12–15], CPW [16–18] and slot-line [19] form.

Here, we show that similar approaches can be applied to cables fabricated on flexible substrates. These can be used to provide interconnects when alternatives such as coaxial cable are inappropriate. One example is medical devices, where a thin-film cable may be sandwiched between a catheter and a surrounding sleeve, leaving internal lumens free for clinical use (e.g. with a guide-wire). Often, only low-frequency or narrow-band operation is required. For example, catheter-based ultrasonic probes operate at very low frequency (5–20 MHz) [20–22], where as detection of magnetic resonance signals involves only marginally higher frequency (63.85 MHz for ^{1}H MRI at 1.5 T). A wide range of magnetic resonance (MR) imaging and tracking catheters have been developed [23–26], increasingly in thin-film form [27, 28].

For microstrip and CPW, dimensions yielding 50 Ω impedances are simple to achieve over small areas on rigid substrates using standard microfabrication, but present difficulties for long cables using PCB processing. For example, microstrip will typically have low impedance when thin (<50 μm) substrates are combined with conductors wide enough (>250 μm) for reliable manufacture. The underlying reason is the small inductance and the large capacitance between conductor and ground. Conversely, CPW has high impedance with comparable conductor separations. However, periodic modification can provide suitable impedance using feature sizes compatible with PCB processing, and thin-film interconnects have recently been used in catheter-based MRI detectors [29]. In this paper, we present a detailed evaluation of periodic cables based on this principle. A simple cable design is introduced in Section 2, and standard theory is used to predict its characteristics. The model is compared with numerical simulation in Section 3. Fabrication and evaluation of prototype cables is described in Section 4, and conclusions are drawn in Section 5.

2 Cable design and analytic model

The aim of this work is to provide a flexible cable, which may be attached to the outside of a catheter using heat-shrink tubing as shown in Fig. 1*a*. Fig. 1*b* shows the cable, which consists of a strip conductor of width w_C and thickness t_C on a dielectric substrate of thickness t_S backed by a ground plane of width w_G and thickness t_G. The ground contains a regular arrangement of rectangular defects, with period a. Each is of width w_D and length $a-b$. In this section, we summarize performance using standard theory.

2.1 Dispersion characteristic

The cable arrangement is diatomic, and in the loss-less case has the lumped-element unit cell marked '0' in Fig. 1*c*. Here L_1 and C_1 are the inductance and capacitance in the defect regions, whereas L_2 and C_2 are the values between.

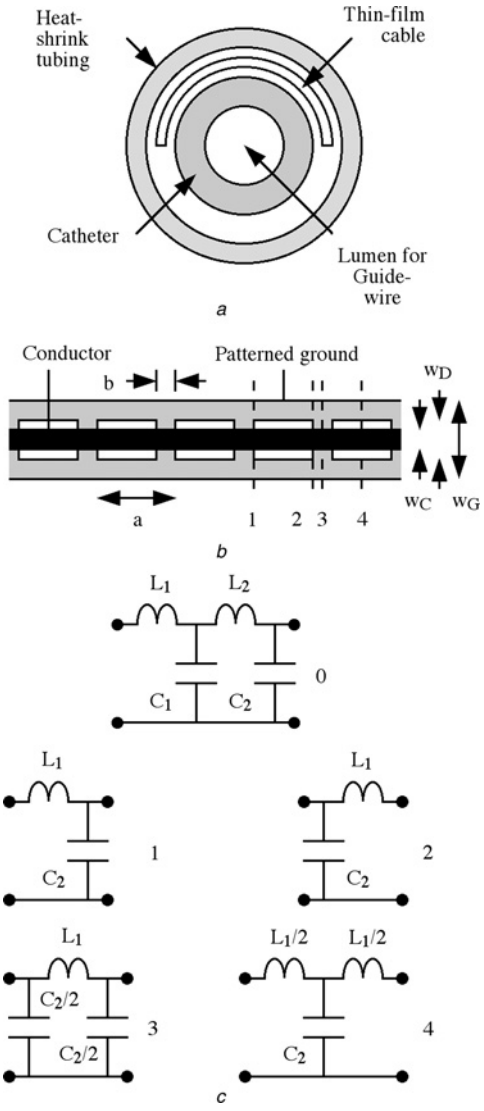

Fig. 1 *Thin-film cable*

a Catheter mounting
b Patterned cable layout, showing different starting points
c Equivalent circuits for diatomic cell starting at position 1 and for monatomic cells starting at positions 1–4

Ignoring fringe fields, these can be approximated using the linear variations $L_1 = L_{p1}(a-b)$, $C_1 = C_{p1}(a-b)$, $L_2 = L_{p2}b$ and $C_2 = C_{p2}b$, where 'p' indicates per-unit-length. The dispersion equation is [8]

$$\omega^4 - \omega^2(1/L_1 + 1/L_2)(1/C_1 + 1/C_2) + (4/L_1L_2C_1C_2)\sin^2(ka/2) = 0 \quad (1)$$

Here, ω is angular frequency and k is the propagation constant. The two solutions are

$$\omega^2 = 1/2\ (1/L_1 + 1/L_2)(1/C_1 + 1/C_2) \pm \sqrt{\left\{ \begin{array}{c} \{1/4\ (1/L_1 + 1/L_2)^2(1/C_1 + 1/C_2)^2 \\ -(4/L_1L_2C_1C_2)\sin^2(ka/2)\} \end{array} \right\}} \quad (2)$$

These solutions form two branches on the ω–k diagram, separated by a gap. The upper (optical) branch is the basis of most PBG filters, whereas the lower (acoustic) branch has been largely neglected. If $L_1 \gg L_2$ and $C_2 \gg C_1$ the solutions approximate to

$$\omega_{\text{acoustic}} = 2\omega_1 \sin(ka/2)$$
$$\omega_{\text{optical}} = \omega_2 - 2(\omega_1^2/\omega_2)\sin^2(ka/2) \quad (3)$$

Here $\omega_1^2 = 1/L_1C_2$, $\omega_2^2 = 1/L_2C_1$ and $\omega_2 \gg \omega_1$. In this case, the branches are well separated, and low-frequency dispersion approximates that of a monatomic lattice. This regime provides low-pass operation up to $\omega_m = 2\omega_1$. Fig. 2*a* compares the exact (thick lines) and approximate (thin lines) dispersion, assuming $L_2/L_1 = C_1/C_2 = 0.1$. There is little difference for the acoustic branch.

2.2 Characteristic impedance

The cable may of course begin at different positions, for example, the dashed lines 1, 2, ..., 4 in Fig. 1*b*. Each has a different unit cell. Cell 1 in Fig. 1*c* can describe a lattice starting at Position 1, whereas Positions 2–4 require Cells 2–4. Although these have the same dispersion, their impedances are given by the different expressions $Z_{C1}, \ldots, Z_{C4}$

$$Z_{C1} = Z_{C0}\exp(-\mathrm{j}ka/2) \qquad Z_{C2} = Z_{C0}\exp(+\mathrm{j}ka/2)$$
$$Z_{C3} = Z_{C0}/\cos(ka/2) \qquad Z_{C4} = Z_{C0}\cos(ka/2) \quad (4)$$

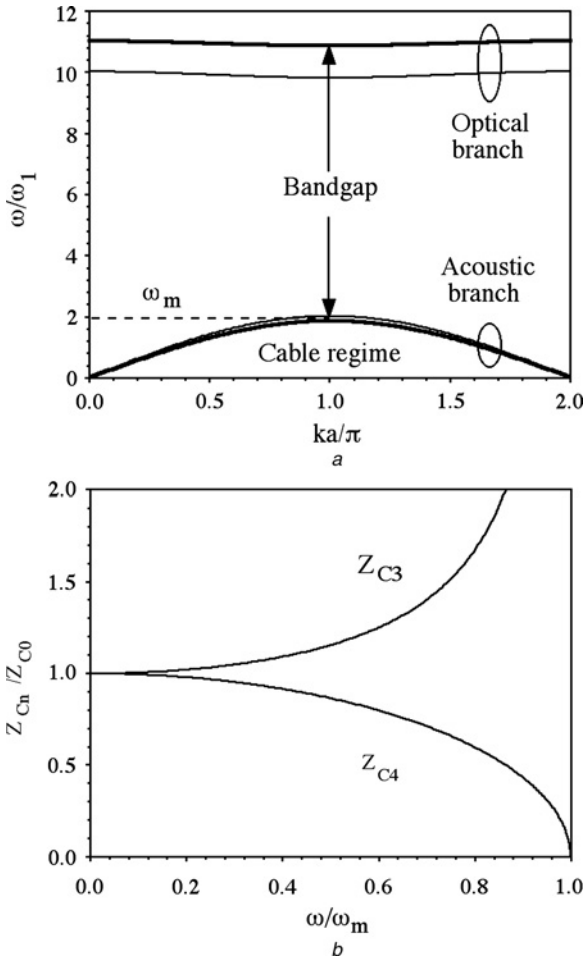

Fig. 2 *Analytic model results*

a Dispersion characteristic, assuming $L_2/L_1 = C_1/C_2 = 0.1$. Thick lines – exact solution, thin lines – approximate solution
b Frequency variation of impedance for patterned cable with unit cells 3 and 4

doi: 10.1049/iet-map.2011.0089

Here, $Z_{C0} = \sqrt{(L_1/C_2)}$ is the impedance at DC. Cells 3 and 4 are of most interest, since they are symmetric and have real impedances. These may be written in terms of ω as

$$Z_{C3} = Z_{C0}/\sqrt{\{1-(\omega/\omega_m)^2\}}$$
$$Z_{C4} = Z_{C0}/\sqrt{\{1-(\omega/\omega_m)^2\}} \quad (5)$$

Fig. 2*b* shows their frequency variations. Owing to the presence of a division sign before the square root, Z_{C3} rises steadily from Z_{C0} to infinity at ω_m, whereas Z_{C4} (which lacks a divisor) reduces to zero. The parameters ω_m and Z_{C0} may be written as

$$\omega_m = 2/\left\{a\sqrt{(L_{p1}C_{p2})}\sqrt{[\beta(1-\beta)]}\right\}$$
$$Z_{C0} = \sqrt{(L_{p1}/C_{p2})}\sqrt{(1/\beta-1)} \quad (6)$$

Here, $\beta = b/a$ is the fractional length of capacitance. Both ω_m and Z_{C0} can be controlled by dimension; ω_m can be very high if a is small, and Z_{C0} increases rapidly as $\beta \to 0$.

Performance is conveniently evaluated in terms of the voltage reflection coefficient between a system with real impedance Z_0 and the patterned cable, namely $R_{Vn} = (Z_{Cn} - Z_0)/(Z_{Cn} + Z_0)$. If the ratio $Z_{CN} = Z_{C0}/Z_0$ is unity, the reflection coefficient $|R_{V3}|$ for Cell 3 will rise from zero at DC to infinity at the band edge. However, if $Z_{CN} < 1$, the reflection is non-zero at DC but can be eliminated at an intermediate frequency ω_M, given by

$$\omega_M/\omega_m = \sqrt{\{1-Z_{CN^2}\}} \quad (7)$$

For $Z_{CN} = 0.85$, for example, $\omega_M/\omega_m \simeq 0.53$. This mechanism can allow exact narrow-band matching at a particular frequency, or extend the frequency range over which $|R_{V3}|$ is lower than a given value. Fig. 3*a* compares the frequency variations of the scattering parameter $S_{11} = 10\log_{10}(|R_{V3}|^2)$ for $Z_{CN} = 1.00$ and 0.85 to illustrate this effect. Similar results can be obtained for Cell 4, with narrow-band matching above DC if $Z_{CN} > 1$.

More generally, a length of cable containing N units may be fed from and terminated by fixed impedance Z_0. In this case, $R_{Vn} = (Z_{in} - Z_0)/(Z_{in} + Z_0)$, where $Z_{in} = Z_{Cn}\{Z_0 + jZ_{Cn}\tan(Nka)\}/\{Z_{Cn} + jZ_0\tan(Nka)\}$. R_{Vn} will now oscillate between the values

$$R_{Vn} = 0, \quad \text{for} \quad ka = \nu\pi/N$$
$$R_{Vn} = (Z_{Cn}^2 - Z_0^2)/(Z_{Cn}^2 + Z_0^2), \quad \text{for} \quad ka = (\nu+1/2)\pi/N \quad (8)$$

Here, ν is an integer. Fig. 3*b* shows the frequency variation of S_{11} for the parameters $N = 20$, $Z_n = 0.85$ and $f_m = 2.25$ GHz, chosen to compare with later results. Quasi-periodic oscillations can be seen, which vanish at $f_M = 1.185$ GHz. Variations of this type allow extraction of the main line parameters, for both numerical and experimental data. For example, the dispersion characteristic can be reconstructed at discrete points from the frequencies of maxima and minima. Similarly, the impedance variation can be reconstructed from the maxima themselves. Once Z_{C0} and ω_m are known, the inductance and capacitance may be found as $L_1 = 2Z_{C0}/\omega_m$ and $C_2 = 2/(Z_{C0}\omega_m)$.

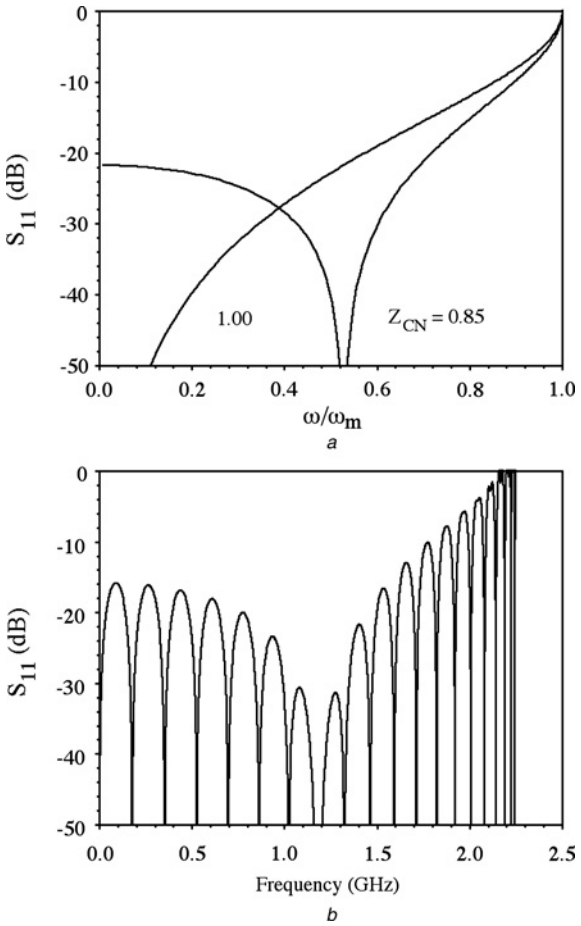

Fig. 3 *Frequency variation of reflection from a junction between conventional and patterned cable*

a Infinite patterned cable with unit cell 3, for different values of Z_{CN}
b Terminated patterned cable for $Z_{CN} = 0.85$ and $f_m = 2.25$ GHz

2.3 Loss

Loss can be modelled by the addition of series resistance R_1 to L_1 and shunt admittance G_2 to C_2. If these are small, the main effect is to introduce propagation loss, whose value may be estimated from a modified dispersion relation. Introducing a complex propagation constant $k = k' - jk''$, it can be shown that k' has the loss-less value whereas k'' is

$$k''a = \omega_0\{R_1C_2 + G_2L_1\}/\{2\cos(k'a/2)\} \quad (9)$$

$k''a$ clearly rises rapidly near the band edge. However, at lower frequencies the cosine may be approximated as unity, so that $k''a \simeq \omega_0\{R_1C_2 + G_2L_1\}/2$. In this regime, frequency dependence arises from the skin effect and dielectric loss and the general variation is complicated. However, if dielectric loss dominates, $k''a \simeq \omega_0G_2L_1/2$. Since $G_2 = \omega C_2\tan(\delta)$, the loss L incurred in a distance d can after substitution for L_1 and C_2 be written as

$$L = 10\omega d\sqrt{(L_{P1}C_{P2})}\sqrt{\{(1-\beta)\beta\}}\tan(\delta)/\log(10)\,\text{dB} \quad (10)$$

In this case, losses are proportional to ω and d, and may conveniently be expressed in units of dB m^{-1} GHz^{-1}. Clearly, losses are low when β is small (when the fractional length of capacitance is small) and also when $\beta \simeq 1$ (however, this is clearly less realistic).

3 Numerical simulation

Detailed modelling is required to verify the assumptions of the previous section and identify suitable geometric parameters. Electromagnetic simulation was therefore carried out using commercial software (Microwave Office, AWR Corp.) using the AXIEM open-boundary non-gridded method-of-moments solver. In this section we describe numerical results.

3.1 Geometric parameters

Parameters were chosen for comparison with later experiments. The period and ground plane width were $a = 16$ mm and $w_G = 4$ mm and the model contained 20 periods of Cell 3. The conductor was assumed to be copper (conductivity $\sigma = 5.96 \times 10^7$ S m^{-1}), with conductor and ground plane thickness $t_C = t_G = 35$ μm. The dielectric was assumed to be polyimide (relative dielectric constant $\varepsilon_{rS} = 3.4$ and loss tangent $\tan(\delta) = 0.005$). Four variants were considered: a dielectric thickness of $t_S = 25$ μm and 50 μm and a conductor width of $w_C = 0.5$ mm (with a defect width of $w_D = 1.5$ mm) and 1 mm (with a defect width of 2 mm). Different values of β were simulated, ranging from unity (continuous microstrip) to 1/64. The upper and lower boundaries were perfect conductors, 30 mm from the model, while the left and right boundaries were open. Port impedances were 50 Ω, and de-embedding was used. Fig. 4*a* shows a typical model, after meshing.

3.2 Loss-less model

Initial simulations were carried out with σ raised artificially by a factor of 10^7 and $\tan(\delta)$ reduced to zero, to simulate loss-less operation. Fig. 4*b* shows a typical frequency variation of S_{11}, for $\beta = 1/4$, $w_D = 2$ mm, $w_C = 1$ mm and $t_S = 25$ μm, which gives a DC impedance and cut-off frequency similar to Fig. 3*b*. The numerical variation is similar and confirms the intermediate null in reflectivity. The figure also shows the variation of S_{21}; the transmission is high until cut-off, when it falls sharply. From these data, the dispersion characteristic and the impedance variation were extracted as described in Section 2. The results agreed well with Fig. 2, thus allowing other parameters to be extracted with confidence.

Fig. 5*a* shows the variation of the DC impedance Z_{C0} with β for the different models. In each case, the impedance rises as β reduces and reaches 50 Ω at a particular value of β. Fig. 5*b* shows the corresponding variations of $f_m = \omega_m/2\pi$ with β. In each case f_m lies in the GHz range. Figs. 6*a* and *b* show the variations of L_1 and C_2 with β. Each varies approximately linearly, L_1 decreasing and C_2 increasing with β. However, the curves flatten at small and large β, respectively, owing to fringe fields. L_1 is almost entirely controlled by the conductor dimensions, and is independent of the substrate thickness. C_2 scales linearly with w_C and inversely with t_S. Similar values of C_2 are therefore obtained for $w_C = 1$ mm, $t_S = 50$ μm and $w_C = 0.5$ mm, $t_S = 25$ μm.

3.3 Lossy model

The conductivity and loss tangent were then re-set to physically realistic values, and calculations were repeated.

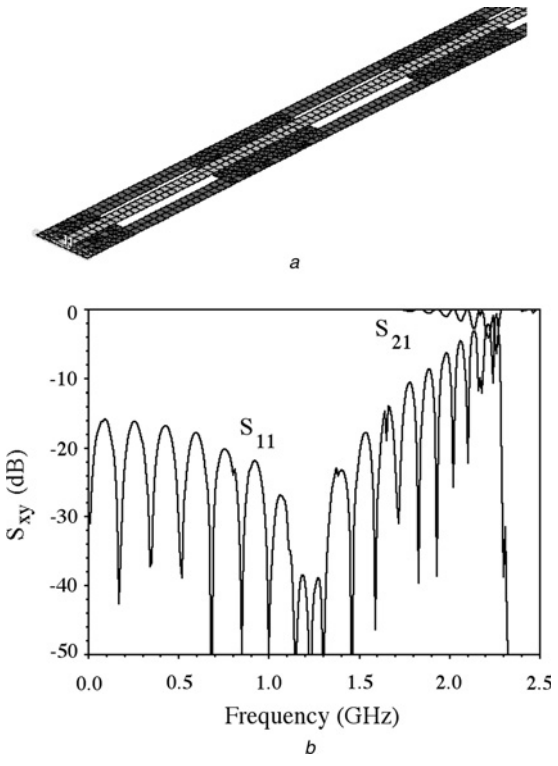

Fig. 4 *EM simulation*

a Simulation model of patterned cable with unit cell 3
b Simulated frequency variation of transmission and reflection, for 20 section cable with $a = 16$ mm, $\beta = 1/4$, $w_G = 4$ mm, $w_D = 2$ mm, $w_C = 1$ mm, $t_S = 25$ μm, $\sigma = 5.96 \times 10^{14}$ S m^{-1} and $\tan(\delta) = 0$

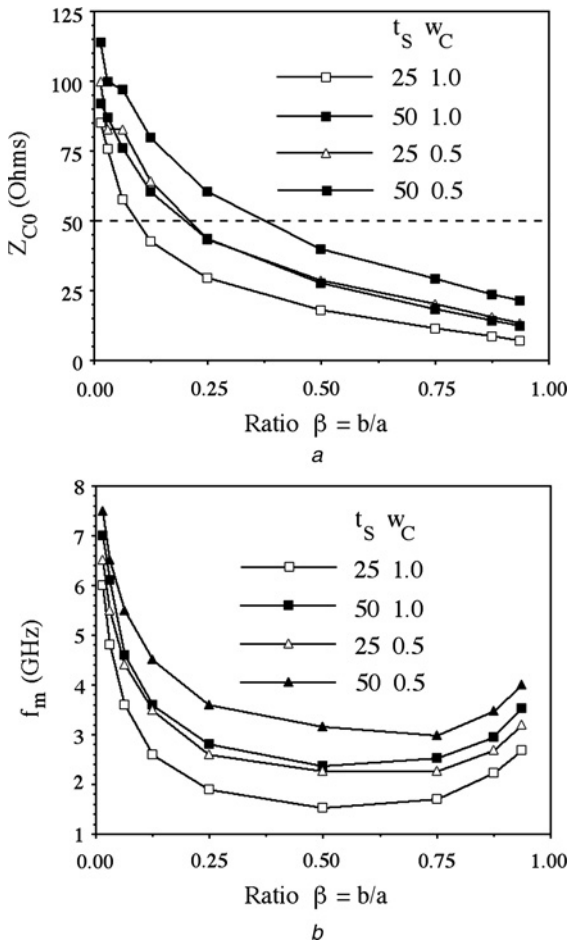

Fig. 5 *Extracted parameter variations with β for patterned cable with unit cell 3*

a Impedance Z_{0D}
b Frequency f_m

doi: 10.1049/iet-map.2011.0089

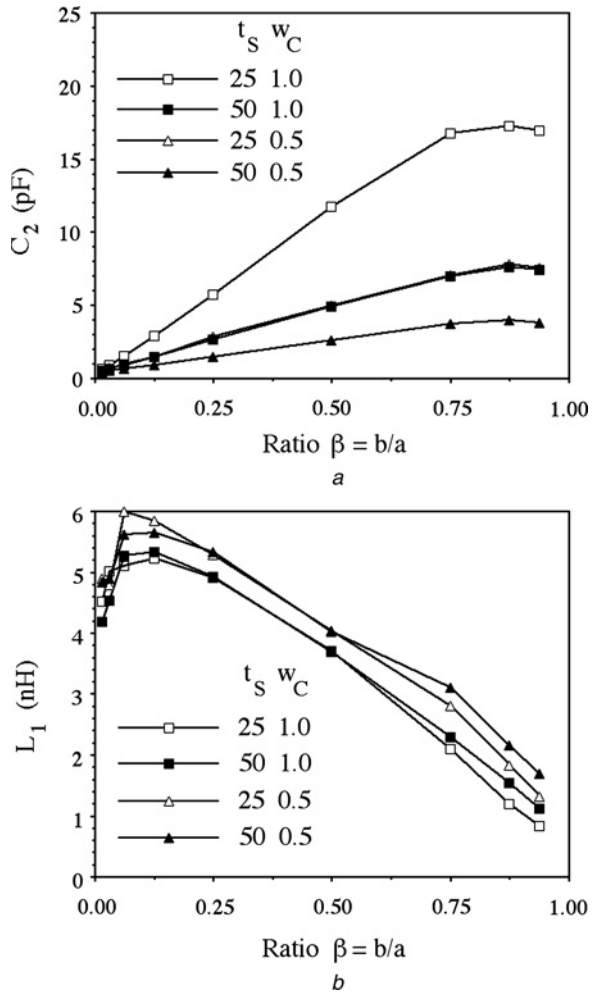

Fig. 6 *Extracted parameter variations with β for patterned cable with unit cell 3*

a Inductance L_1
b Capacitance C_2

The effect of loss is to reduce the fringe contrast in the variation of S_{11}, to introduce an approximately linear dependence of loss on frequency in the variation of S_{21} below cut-off and to render the cut-off less abrupt. The propagation loss was then extracted in units of dB m^{-1} GHz^{-1}. With dielectric loss alone, variations were qualitatively similar to (10) for $\beta < 0.5$, but discrepancies suggested that very long lines (which had very long simulation times) would be needed to obtain accurate results.

4 Experimental verification

Prototype cables were fabricated in 2 m lengths by the UK company Clarydon (Willenhall, West Midlands). The starting material was copper-clad polyimide (Kapton® HN, DuPont High Performance Films) [30]. In this section we describe design and performance.

4.1 Design and fabrication

Kapton thicknesses of $t_S = 25$ μm and $t_S = 50$ μm were used, each with a copper thickness $t_C = t_G = 35$ μm. Seven values of β (1, 1/2, 1/4, 1/8, 1/16, 1/32 and 1/64) were investigated. The first corresponds to uniform microstrip and the others to periodic lines. Two conductor widths were used: $w_C = 1$ mm with a defect width of $w_D = 2$ mm and $w_C = 0.5$ mm with $w_D = 1.5$ mm. The ground plane width was $w_G = 4$ mm, and the period was $a = 16$ mm, and so each line contained 125 periods. Fig. 7*a* shows the fabrication process. Patterning was carried out using stepped double-sided exposure to 1 m long photo-masks formed from Mylar-coated silver halide on polyester. Each side of the PCB (i) was first coated with a 175 μm thick layer of laminated photoresist. (ii) The sensitised PCB was then sandwiched between the two photo-masks on a glass backing, using pins for alignment. Each side of the PCB was exposed with a UV lamp, and the process was repeated in a second exposure. (iii) Resist development and metal etching were carried out with the PCB horizontal. (iv) The resist was then stripped. (v) Lines were fabricated in arrays and separated using a scalpel. Fig. 7*b* shows a completed cable, before and after mounting on a 2.66 mm dia (8 Fr) catheter.

4.2 Evaluation

Cables were terminated with SMA connectors in the arrangement of Cell 3, and characterisation was carried out using an Agilent electronic network analyser with the cable in a *U*-shaped loop. There was little difference between the performance of flat and catheter-mounted cable, but periodically patterned cable outperformed uniform microstrip. Figs. 8*a* and *b* compare the frequency variation of the scattering parameters S_{21} and S_{11} for different cables. Each has a substrate thickness of 25 μm and a strip width of 0.5 mm. Uniform microstrip has high propagation loss, and its transmission decreases rapidly with frequency. This cable also generates a large reflection, but S_{11} settles to a

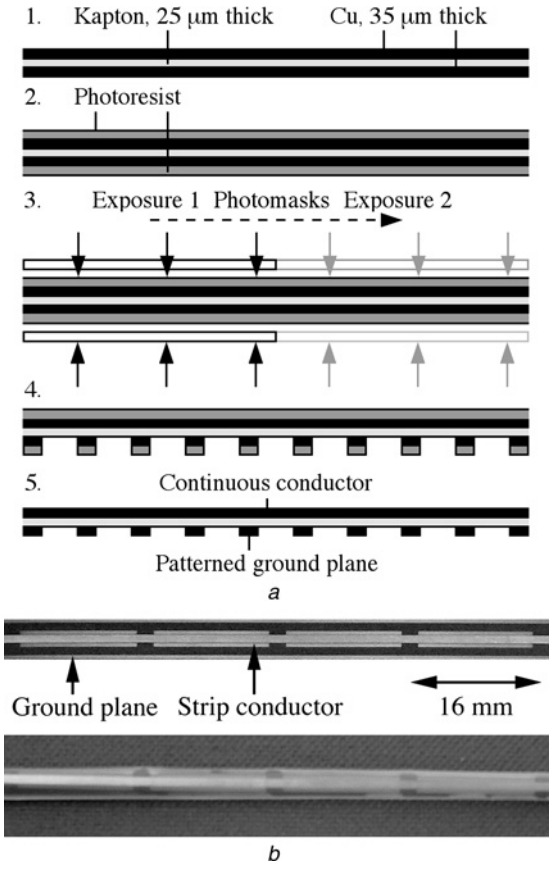

Fig. 7 *Experimental cable*

a Thin-film cable fabrication process
b Completed patterned cable, before and after mounting on catheter

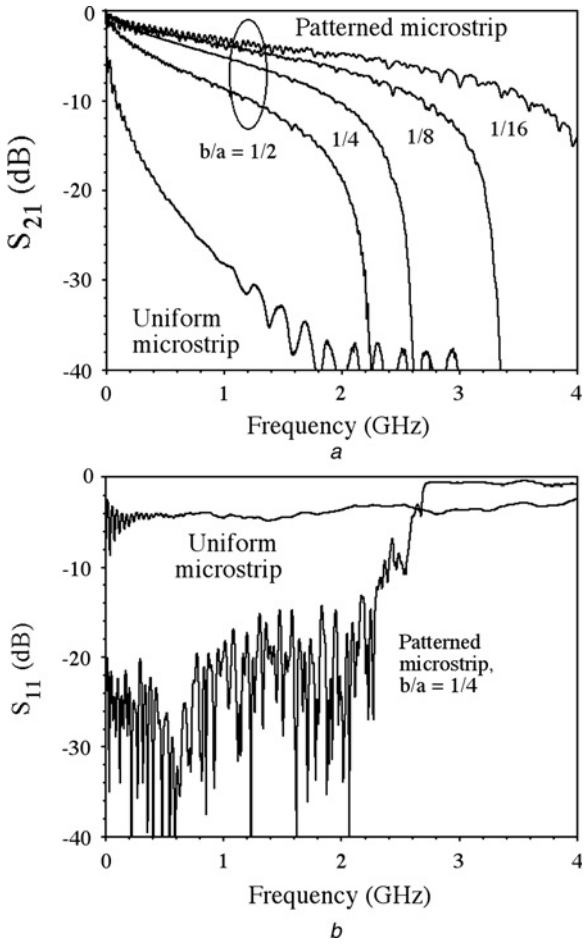

Fig. 8 *Experimental frequency variation of scattering parameters for uniform microstrip and patterned cables with unit cell 3*

a S_{21}
b S_{11}

steady value after some initial oscillations because of multiple internal reflections. Propagation loss for periodically patterned cable is much lower, at least up to cut-off, which lies in the range of 2.2–4.3 GHz for the cables shown. At this point, S_{21} decreases rapidly. For the patterned cable in Fig. 8*b*, reflection at DC is low, but rises near cut-off after a minimum near 0.6 GHz owing to the narrow-band impedance matching described in Section 2.

For uniform microstrip, Z_0 was found from the high-frequency value of S_{11} when multiple reflections can be ignored. For periodic lines, Z_{C0} was found as described in Section 2. Fig. 9*a* shows the variation of Z_{C0} with β for all types of line. For large β, the DC characteristic impedance is generally less than 50 Ω. However, a decrease in β causes a steady increase in Z_{C0}, and for each combination of t_S and w_C there is a value of β that allows matching to 50 Ω. These results are in good agreement with Fig. 5*a*. Propagation losses were estimated from regions where transmission varies quasi-linearly with frequency, and the results are shown in Fig. 9*b* in units of dB m^{-1} GHz^{-1}. The loss varies qualitatively as predicted by (10) for small β. In this regime, L is a few dB m^{-1} GHz^{-1}, making the losses negligible up to 100 MHz. The best overall performance was obtained using narrow (0.5 mm) conductors on thin (0.25 μm) substrates. For this case, 50 Ω impedance would be obtained for $\beta \simeq 0.3$. These results confirm that impedance control may be combined with low loss in thin-film microstrip cable using periodic patterning.

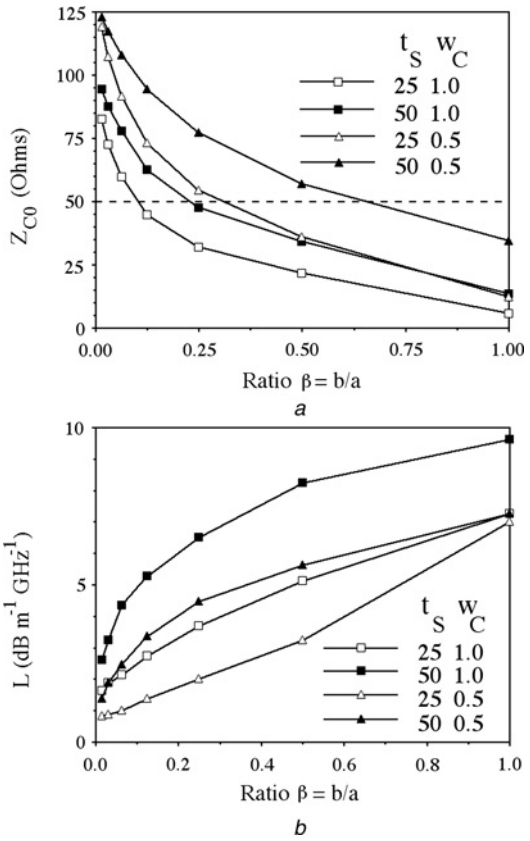

Fig. 9 *Extracted parameter variation with β for patterned cables with unit cell 3*

a Impedance Z_{C0}
b Loss L

5 Conclusions

We have shown that periodic patterning of a thin-film waveguide allows the construction of flexible cables with controllable properties. Numerical simulations have verified the predictions of a simple analytic model. Cables have been fabricated in 2 m lengths using copper-clad polyimide, and DC characteristic impedances close to 50 Ω have been combined with low propagation loss. This initial result suggests that periodic cables could provide flexible interconnects in applications where space is at a premium or conventional packaging is difficult. A similar adjustment of low-frequency impedance can be achieved by periodically loading a CPW with thin-film capacitors. Similar techniques may also be used to form thin-film cables with other useful properties. Examples include band-pass or high-pass characteristics, to avoid a DC connection in safety-critical applications. Patterning may also be used to form spatially varying structures (for example, to provide a distributed impedance transformation) and to incorporate additional lumped-element splitters and filters.

6 Acknowledgment

The authors are extremely grateful to Mr John Barry of Clarydon for cable fabrication.

7 References

1 Grieg, D.D., Engelmann, H.F.: 'Microstrip – a new transmission technique for the kilomegacycle range', *Proc. I.R.E.*, 1952, **40**, (12), pp. 1644–1650

2 Wen, C.P.: 'Coplanar waveguide: a surface strip transmission line suitable for nonreciprocal gyromagnetic device applications', *IEEE Trans. Microw. Theory Tech.*, 1969, **MTT-17**, (12), pp. 1087–1990
3 Cohn, S.B.: 'Slot line on a dielectric substrate', *IEEE Trans. Microw. Theory Tech.*, 1969, **MTT-17**, (10), pp. 768–778
4 Wheeler, H.A.: 'Transmission-line properties of a strip on a dielectric sheet on a plane', *IEEE Trans. Microw. Theory Tech.*, 1977, **MTT-25**, (8), pp. 631–647
5 Hirota, T., Minakawa, A., Muraguchi, M.: 'Reduced-size branch-line and rat-race hybrids for uniplanar MMICs', *IEEE Trans. Microw. Theory Tech.*, 1990, **38**, (3), pp. 270–275
6 Lim, J.-S., Park, J.-S., Lee, Y.-T., Ahn, D., Nam, S.: 'Application of defected ground structure in reducing the size of amplifiers', *IEEE Microw. Wirel. Compon. Lett.*, 2002, **12**, (7), pp. 261–263
7 Schnieder, F., Doerner, R., Heinrich, W.: 'High impedance coplanar waveguides with low attenuation', *IEEE Microw. Guid. Wave Lett.*, 1996, **6**, (3), pp. 117–119
8 Brillouin, L.: 'Wave propagation in periodic structures' (Dover Publications, 1953, 2nd edn.)
9 Nair, N.V., Mallick, K.: 'An analysis of a width-modulated microstrip periodic structure', *IEEE Trans. Microw. Theory Tech.*, 1984, **MTT-2**, (2), pp. 200–204
10 Glandorf, F., Wolff, I.: 'A spectral domain analysis of periodically nonuniform microstrip lines', *IEEE Trans. Microw. Theory Tech.*, 1987, **MTT-35**, (3), pp. 336–343
11 Kahrizi, M., Sarkar, T.K., Maricevic, Z.A.: 'Dynamic analysis of a microstrip line over a perforated ground plane', *IEEE Trans. Microw. Theory. Tech.*, 1994, **42**, (5), pp. 820–825
12 Radisic, V., Qian, Y., Coccioli, R., Itoh, T.: 'Novel 2-D photonic bandgap structure for microstrip lines', *IEEE Microw. Guid. Wave Lett.*, 1998, **8**, (2), pp. 60–71
13 Rumsey, I., Piket-May, M., Kelly, P.-K.: 'Photonic bandgap structures used as filters in microstrip circuits', *IEEE Microw. Guid Wave Lett.*, 1998, **8**, (10), pp. 336–338
14 Yang, F.R., Qian, Y., Coccioli, R., Itoh, T.: 'A novel low-loss slow-wave microstrip structure', *IEEE Microw. Guid. Wave Lett.*, 1998, **8**, (11), pp. 372–374
15 Falcone, F., Lopetegi, T., Sorolla, M.: '1-D and 2-D photonic bandgap structures', *Microw. Opt. Technol. Lett.*, 1999, **22**, (6), pp. 411–412
16 Gorur, A., Karpuz, C., Alkan, M.: 'Characteristics of a periodically loaded CPW structure', *IEEE Microw. Guid. Wave Lett.*, 1998, **8**, (8), pp. 278–280
17 Sor, J., Qian, Y., Itoh, T.: 'Miniature low-loss CPW periodic structures for filter applications', *IEEE Trans. Microw. Theory Tech.*, 2001, **49**, (12), pp. 2336–2341
18 Zhu, L.: 'Guided-wave characteristics of periodic coplanar waveguides with inductive loading – unit length transmission parameters', *IEEE Trans. Microw. Theory Tech.*, 2003, **51**, (10), pp. 2133–2138
19 Yun, T.-Y., Chang, K.: 'Uniplanar one-dimensional photonic bandgap structures and resonators', *IEEE Trans. Microw. Theory Tech.*, 2001, **49**, (3), pp. 549–553
20 Bom, N., Lancee, C.T., Van Egmond, F.C.: 'An ultrasonic intracardiac scanner', *Ultrasonics*, 1972, **10**, (2), pp. 72–77
21 Bom, N., ten Hoff, H., Lancée, C.T., Gussenhoven, W.J., Bosch, J.G.: 'Early and recent intraluminal ultrasound devices', *Int. J. Cardiac. Imag.*, 1989, **4**, (2–4), pp. 79–88
22 Yock, P.G., Linker, D.T.: 'Intravascular ultrasound. Looking below the surface of vascular disease', *Circulation*, 1990, **81**, (5), pp. 1715–1718
23 Kantor, H.L., Briggs, R.W., Balaban, R.S.: 'In vivo ^{31}P nuclear magnetic resonance measurements in canine heart using a catheter-coil', *Circ. Res.*, 1984, **55**, (2), pp. 261–266
24 Hurst, G.C., Hua, J., Duerk, J.L., Cohen, A.M.: 'Intravascular (catheter) NMR receiver probe: preliminary design analysis and application to canine iliofemoral imaging', *Magn. Reson. Med.*, 1992, **24**, (2), pp. 343–357
25 Hillenbrand, C.M., Elgort, D.R., Wong, E.Y., *et al.*: 'Active device tracking and high-resolution intravascular MRI using a novel catheter-based opposed solenoid phased array coil', *Magn. Reson. Med.*, 2004, **51**, (4), pp. 668–675
26 Zuehlsdorff, S., Umathum, R., Volz, S., *et al.*: 'MR coil design for simultaneous tip tracking and curvature delineation of a catheter', *Magn. Reson. Med.*, 2004, **52**, (1), pp. 214–218
27 Woytasik, M., Ginefri, J.-C., Raynaud, J.-S., *et al.*: 'Characterisation of flexible RF microcoils dedicated to local MRI', *Microsyst. Technol.*, 2007, **13**, (11–12), pp. 1575–1580
28 Ahmad, M.M., Syms, R.R.A., Young, I.R., *et al.*: 'Catheter-based flexible microcoil RF detectors for internal magnetic resonance imaging', *J. Micromech. Microeng.*, 2009, **19**, (7), article id 074011
29 Syms, R.R.A., Young, I.R., Ahmad, M.M., Rea, M., Wadsworth, C.A., Taylor-Robinson, S.-D.: 'Thin-film detector system for internal magnetic resonance imaging', *Sens. Actuators A*, 2010, **163**, (1), pp. 15–24
30 Dupont Kapton® HN Polyimide Film Data Sheet K-15345, 2006